SIAM J. APPL. MATH.
Vol. 61, No. 5, pp. 1578–1604

PROPAGATING ACTIVITY PATTERNS IN THALAMIC NEURONAL NETWORKS*

D. H. TERMAN†, G. B. ERMENTROUT‡, AND A. C. YEW†

Abstract. Singular perturbation methods are used to construct traveling waves for models of thalamic networks. We first study a single layer of mutually inhibitory neurons, each of which has the ability to rebound after hyperpolarization. Two types of waves are constructed: smoothly propagating waves and lurching waves which propagate in a saltatory fashion. We reduce the existence of these waves to simple boundary value problems or algebraic systems which are solved using the computational package AUTO. The resulting calculations are compared to numerical simulations of the network. Finally, some comments are made concerning two-layer networks.

Key words. singular perturbation, traveling waves, synaptic coupling, inhibition

AMS subject classifications. 92C20, 34C15, 34C26, 45J05

PII. S0036139999365092

1. Introduction.

A number of computational models have been developed with the aim of understanding the mechanisms of wave propagation in networks of neurons in thalamic slice preparations [3, 4, 5, 7, 12, 14]. The slice preparation was developed by McCormick and his collaborators in order to study various rhythms that underlie sleep and are believed to originate in the thalamus [1, 2, 9, 10, 11, 14]. The computational models typically consist of two layers of neurons: the thalamocortical (TC) cells and the reticularis (RE) cells. The TC cells are excitatory and project to both the cortex and the RE cells. The RE cells are inhibitory and project to other RE cells as well as to TC cells (see the circuit in Figure 1). Both cell types have various ionic currents that are responsible for their properties, but the dominant current and the one that gives rise to their interesting properties is the so-called T-current. The T-current is produced by the influx of calcium ions and leads to a large depolarization of the membrane on which spikes generated by other fast currents ride. These bursts of action potentials are observed both in models and in intracellular recordings of the cells. The T-current (depending on parameters) operates in two different modes. In the *excitable* mode, a brief depolarization results in a burst of action potentials from the cell. In the *rebound* mode, the cell must be hyperpolarized (brought to a potential more negative than rest) and then released from the inhibition before it can fire a burst of action potentials. In some modeling studies [8] the TC cells have the rebound property and the RE cells have the excitable property. Thus, the propagation of activity is mediated as follows. A burst of TC cells excites neighboring RE cells causing them to fire. This in turn inhibits neighboring TC cells. When the inhibition wears off, the TC cells rebound with a burst which continues the process along the tissue.

In a recent paper, Rinzel et al. [12] considered a simplification of this circuit. By

*Received by the editors December 13, 1999; accepted for publication (in revised form) August 22, 2000; published electronically February 2, 2001.
http://www.siam.org/journals/siap/61-5/36509.html
†Department of Mathematics, Ohio State University, Columbus, OH 43210 (terman@math.ohio-state.edu, yew@math.ohio-state.edu). The research of the first author was supported in part by NSF grant DMS-9802339.
‡Department of Mathematics, University of Pittsburgh, Pittsburgh, PA 15260 (bard@pitt.edu). The research of this author was supported in part by NSF grant DMS-9972913.

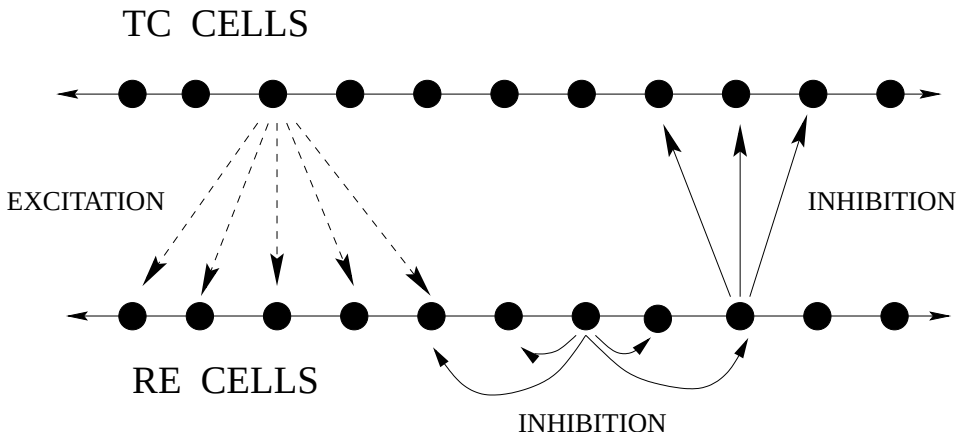

FIG. 1. *Two-layered network of TC cells and RE cells. The TC cells excite the RE cells. The RE cells send inhibition back to the TC cells and also inhibit each other.*

endowing the RE cells with the rebound property, they reduced the two-layered network to one layer which is able to produce propagating waves. The feature that makes these waves interesting from a mathematical point of view is that they do not travel in a smooth fashion, but rather have a saltatory, or "lurching," quality. Experimentally, it is not known whether the waves in the slice lurch since the spatial measurements of the membrane potential are not sufficiently fine to discriminate variations in the velocity due to heterogeneities from actual dynamic lurching. However, many of the computational models have this lurching property. Rinzel et al. also made the following observation. If the coupling had a local gap (e.g., cells were not coupled locally but were coupled at some distance from the center), then smooth propagation occurs.

Golomb and Ermentrout [7] have recently used a simple integrate and fire model with conductance delays to study the difference between smooth and lurching waves. They find that as the coupling delay between neurons increases, the smoothly propagating wave becomes unstable and lurching waves arise. The coupling gap in the work of Rinzel et al. essentially allows cells to escape from inhibition sooner so that this "delay" is shorter and smooth waves result.

In this paper, we explore the biophysical equations used in Rinzel et al. [12] as well as in [8] and study the existence of smooth and lurching waves using singular perturbation theory. Instead of the model considered in [7] we study the full network equations. Using geometric singular perturbation methods, we derive explicit formulas for when a particular type of wave exists. These formulas also determine how the velocity of the waves depends on network parameters. As we shall see, each type of wave may leave a variety of different sorts of activity patterns in its wake. The geometric methods we develop are very useful in understanding the mechanisms responsible for these different patterns.

In the next section, we lay out the model. Various types of activity patterns we observed in the full two-layer network are described in section 3, followed by an introduction to basic singular analysis methods in section 4. Sections 5 and 6 contain the bulk of the paper, where we analyze the smooth and lurching waves for one-layer networks. The discussion in section 7 contains comparisons of various models and results, as well as some open problems.

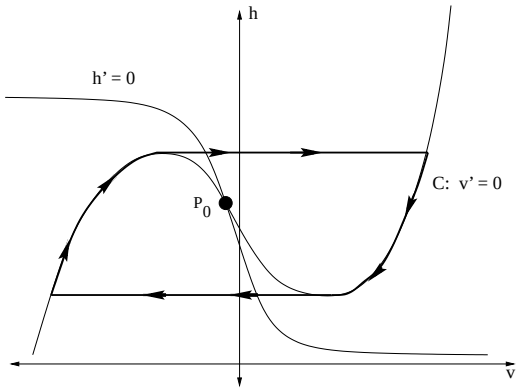

FIG. 2. *Nullclines corresponding to a single oscillatory cell. The bold curve represents the singular periodic solution (limit cycle).*

2. The model.

2.1. Single cell. In the numerical simulations, individual cells satisfy differential equations of the form

$$\begin{aligned} C_m v' &= -g_L(v - v_L) - g_{Ca} m_\infty(v) h(v - v_{Ca}), \\ h' &= \epsilon(h_\infty(v) - h)/\tau_h(v). \end{aligned} \tag{2.1}$$

These equations arise as reduced models for thalamic neurons; see, for example, [8, 12]. The definitions of the nonlinear functions and parameters in (2.1) are given in the appendix. The results do not, however, depend on the precise details of the equations. For this reason, we usually write (2.1) as

$$\begin{aligned} v' &= f(v, h), \\ h' &= \epsilon(h_\infty(v) - h)/\tau_h(v). \end{aligned} \tag{2.2}$$

The following assumptions on the nonlinear functions in (2.2) will be needed for the analysis: We assume that the v-nullcline $\{f = 0\}$ represents a cubic-shaped curve, denoted by C, as in Figure 2. We further assume that $v' > 0$ (< 0) above (below) C. The h-nullcline $\{h = h_\infty(v)\}$ is taken to be a nonincreasing curve that intersects C at a unique point, which we denote by $p_0 = (v_0, h_0)$. Moreover, $\tau_h(v)$ is assumed to be positive and nonincreasing; it then follows that $h' > 0$ (< 0) below (above) the h-nullcline. If p_0 lies on the left branch of C, then (2.2) is said to be *excitable*; in this case p_0 is a globally stable fixed point of (2.2). If p_0 lies on the middle branch of C, then (2.2) is said to be *oscillatory*; (2.2) will then exhibit a stable limit cycle when ϵ is small.

2.2. Synaptic coupling. We model two mutually coupled cells as

$$\begin{aligned} v_i' &= f(v_i, h_i) - g_{syn} s_j (v_i - v_{syn}), \\ h_i' &= \epsilon(h_\infty(v_i) - h_i)/\tau_h(v_i), \\ s_i' &= \alpha(1 - s_i) H(v_i - \theta) - \epsilon\beta s_i. \end{aligned}$$

Here, $i, j = 1, 2$ and $i \neq j$. The constants α, β, and g_{syn} are all positive and H is the Heaviside step function. Hence, θ is a threshold above which the presynaptic cell

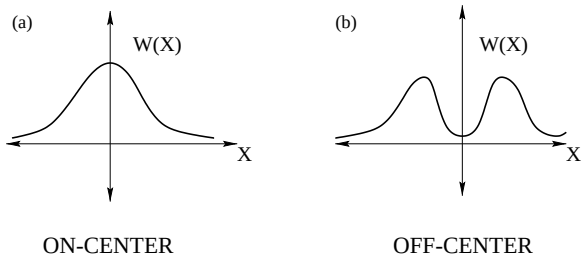

FIG. 3. *Examples of two different types of synaptic footprint:* (a) *on-centered and* (b) *off-centered.*

j must be to activate the synaptic variable s_j. If $v_j < \theta$, then s_j decays slowly to 0 (deactivates) at the rate $\epsilon\beta$. On the other hand, if $v_j > \theta$, then s_j activates with rate $\alpha + \epsilon\beta$ which is $O(1)$ with respect to ϵ. Our choice of synaptic turn-on and turn-off rates is motivated by models for thalamic sleep rhythms. The synapses are said to be *excitatory* if the reversal potential v_{syn} satisfies $v_{syn} > v_0$, and *inhibitory* if $v_{syn} < v_0$.

2.3. Architecture. We consider one-dimensional arrays of cells. The network may be single layered or double layered. A single-layered network is modeled as

$$\begin{aligned} v_i' &= f(v_i, h_i) - \frac{g_{syn}}{N}(v_i - v_{syn}) \sum_j W_{ij} s_j, \\ h_i' &= \epsilon(h_\infty(v_i) - h_i)/\tau_h(v_i), \\ s_i' &= \alpha(1 - s_i)H(v_i - \theta) - \epsilon\beta s_i. \end{aligned} \tag{2.3}$$

Here, N is the total number of cells in the network, the sum is over all the cells in the network, and W_{ij} represents a synaptic weight; it can be viewed as the probability that there is a synaptic connection between cell j and cell i. We assume that W_{ij} is of the form $W_{ij} = W(i-j)$, where $W(x)$ is a positive, even function, often referred to as the "synaptic footprint." Figure 3 shows two possible choices for $W(x)$. In Figure 3(a), $W(x)$ has a maximum at $x = 0$ and is decreasing for $x > 0$. This is referred to as *on-centered* connectivity. In Figure 3(b), the connectivity is *off-centered*, where $W(x)$ is small for x small and has a maximum at some $x_0 > 0$.

For the analysis it will be convenient to consider a continuum limit as the number of cells becomes unbounded. We are then led to consider the integral-differential equation

$$\begin{aligned} v_t &= f(v, h) - g_{syn}(v - v_{syn}) \int_{-\infty}^{\infty} W(x - y) s(y, t) dy, \\ h_t &= \epsilon(h_\infty(v) - h)/\tau_h(v), \\ s_t &= \alpha(1 - s)H(v - \theta) - \epsilon\beta s, \end{aligned} \tag{2.4}$$

where (v, h, s) are functions of (x, t).

We shall also briefly discuss two-layered networks, as illustrated in Figure 1. The different layers represent thalamocortical relay (TC) and thalamic reticularis (RE) cells. The TC cells send excitation to the RE cells, while the RE cells send inhibitory coupling both to the TC cells and to other RE cells. We do not present the full equations for this network here; more information can be found in the appendix.

3. Numerical results. To illustrate the numerous types of propagating patterns, here we describe some results obtained from numerical simulations of the full

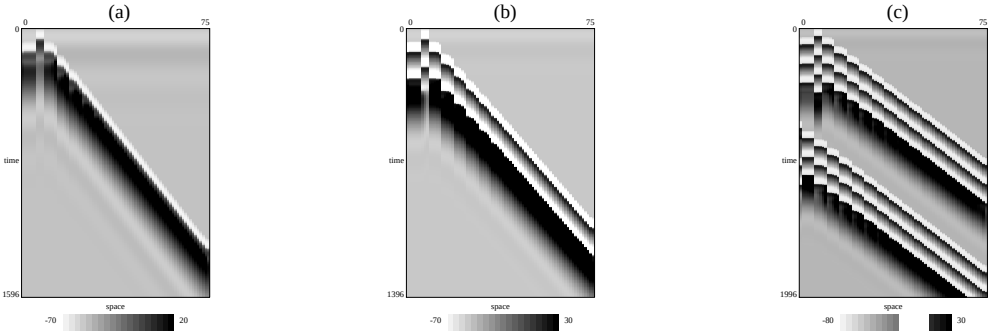

FIG. 4. *Smooth waves for a two-layered network:* (a) *a solitary pulse,* (b) *a double pulse,* (c) *a multiple pulse solution. Parameter values corresponding to each wave are given in the appendix.*

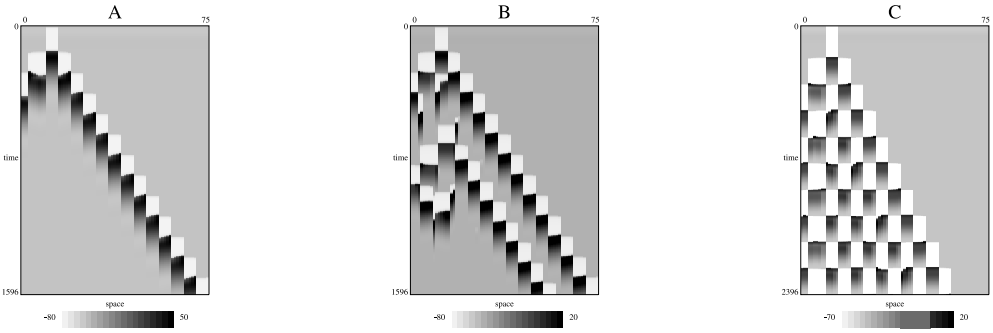

FIG. 5. *Lurching waves for a two-layered network:* (a) *a solitary lurcher,* (b) *a double lurcher,* (c) *a lurching wave with periodic clustering in the wake. Parameter values corresponding to each wave are given in the appendix.*

two-layered network. Two general classes of waves are observed, which we refer to as *smooth waves* and *lurching waves*. A smooth wave corresponds to a fixed profile moving with constant velocity, much like a single action potential traveling down a nerve axon. If we keep track of the spatial positions x and the times t for which the leading edge of the membrane potential is at some fixed value, then this defines a straight line of the form $x - \mu t =$ constant, where the slope μ corresponds to the wave speed.

Several types of smooth waves are shown in Figure 4. Parameter values are given in the appendix. A solitary pulse is illustrated in Figure 4(a). Multiple pulses may also exist, and a double pulse is shown in Figure 4(b). There may also exist periodic smooth wave trains. Finally, a more exotic smooth wave is shown in Figure 4(c); three bursts at a frequency of about 6–7 Hz are followed by a silent period of about 200 ms, and this is then followed by another sequence of three bursts.

A lurching wave does not propagate with constant velocity. Instead, the propagating wave recruits groups or clusters of cells in discrete steps. The leading edge of active cells inhibits some cluster of cells ahead of it; the size of this cluster depends on the synaptic footprint. Inhibited cells must wait until the active cells fall back to the silent phase, and then for inhibition to wear off, before they are able to jump up to the active phase.

Several types of lurching waves are illustrated in Figure 5. There may exist single

and multiple lurching pulses as shown in Figures 5(a) and (b). For each of these solutions, the network eventually returns to rest in the wake of the propagating wave. The network may, however, also exhibit sustained oscillations. Cells in the wake of the wave may oscillate synchronously, or they may form clusters as shown in Figure 5(c). The firing of cells within each cluster is nearly synchronous, while different clusters are desynchronized. The activity patterns in the wake of the wave may also be quite complicated and disorganized.

4. Introduction to the analysis.

4.1. Singular solutions. It is instructive to consider simple networks before discussing large arrays of oscillators and population dynamics. To introduce our basic approach for analyzing the models in section 2, it is important to first understand the intrinsic dynamics of a single cell and how an individual cell responds to synaptic input from another cell.

All of the solutions discussed in this paper are analyzed using a geometric singular perturbation approach. The parameter ϵ is taken to be small, which allows us to dissect the full equations into fast and slow subsystems and then construct "*singular solutions*" of the equations in which ϵ is formally set equal to zero. The singular solutions typically consist of several pieces; each piece is a solution of one of the reduced fast or slow subsystems. These singular constructions enable us to derive formulas for when a particular solution is likely to exist, what bifurcations of the solutions might take place as parameters are varied, and how properties such as the wave speed depend on parameters.

The basic idea behind our approach is most simply illustrated by considering a single oscillatory cell without any synaptic input. Recall that such a cell satisfies (2.2), and since it is oscillatory, the fixed point p_0 lies on the middle branch of the cubic-shaped nullcline C. The system (2.2) then gives rise to a limit cycle which approaches the singular solution shown in Figure 2 as $\epsilon \to 0$. This singular solution consists of four pieces. The silent and active phases correspond to the pieces on the left and right branches of C, respectively. These pieces satisfy slow equations which we will define shortly. The two remaining pieces are transitions between the silent and active phases; they correspond to the jump-up and jump-down between the left and right branches of C and are governed by fast equations.

The fast equations are obtained by simply setting $\epsilon = 0$ in (2.2). Note that h is then constant and v satisfies a scalar equation. The slow equations are obtained by introducing the slow time $\tau = \epsilon t$ in (2.2) and then letting $\epsilon = 0$. This leads to

$$\begin{aligned} 0 &= f(v,h), \\ \dot{h} &= (h_\infty(v) - h)/\tau_h(v), \end{aligned} \tag{4.1}$$

where differentiation is with respect to τ. These equations tell us that (v,h) lies on C with the evolution along C given by the second equation in (4.1).

It will be convenient to introduce the following notation. Let $\mathcal{C}_S$, with $0 < S < 1$, denote the curve $\{(v,h) : f(v,h) - g_{syn}S(v - v_{syn}) = 0\}$. These curves are cubic shaped as long as g_{syn} is not too large. We denote the left and right knees of $\mathcal{C}_S$ by $(v_{LK}(S), h_{LK}(S))$ and $(v_{RK}(S), h_{RK}(S))$, respectively. Let $P_{FP}(S) = (v_{FP}(S), h_{FP}(S))$ be the point of intersection of $\mathcal{C}_S$ and the h-nullcline $\{h = h_\infty(v)\}$. This is a fixed point for each cell if the synaptic input is held constant at the level S. We say that $\mathcal{C}_S$ is excitable (oscillatory) if $(v_{FP}(S), h_{FP}(S))$ lies on the left (middle) branch of $\mathcal{C}_S$. Throughout the analyses that follow, it will be assumed that each cell

without any input is excitable; hence, $\mathcal{C}_0$ is excitable. It is possible, however, that $\mathcal{C}_S$ is oscillatory for some other levels of synaptic input S. As we shall see, this may have an important impact on the types of waves that emerge. We remark that for excitatory coupling, $\mathcal{C}_S$ lies below $\mathcal{C}_0$, and for inhibitory coupling, $\mathcal{C}_S$ lies above $\mathcal{C}_0$.

In larger networks, the cells will still lie on the left branch of some cubic during the silent phase and on the right branch of possibly another cubic during the active phase. Which cubic the cell lies on is determined by the level of synaptic input the cell receives.

4.2. When does one cell fire in response to another? Here we consider the simple network consisting of a pair of cells with cell 2 receiving synaptic input from cell 1. We assume that cell 1 fires an action potential burst and describe the possible responses of cell 2. In particular, we find conditions on the parameters for whether or not cell 2 also fires a burst.

Now cell 2 evolves according to the equations

$$\begin{aligned} v_2' &= f(v_2, h_2) - g_{syn} s_1 (v_2 - v_{syn}), \\ h_2' &= \epsilon (h_\infty(v_2) - h_2)/\tau_h(v_2), \end{aligned} \tag{4.2}$$

where $s_1(t)$ satisfies the scalar equation

$$s_1' \;=\; \alpha(1 - s_1) H(v_1 - \theta) - \epsilon \beta s_1.$$

In the following discussion, we will work with the slow equations (i.e., change the independent variable to $\tau = \epsilon t$) and view the jumps up and down as instantaneous. Assume that cell 1 fires at $\tau = 0$ and remains active for $0 < \tau < T_0$; that is, $v_1 > \theta$ for $0 < \tau < T_0$. It then follows that in the limit $\epsilon \to 0$,

$$s_1(\tau) \;=\; \begin{cases} 1 & \text{for} \quad 0 < \tau < T_0, \\ e^{-\beta(\tau - T_0)} & \text{for} \quad \tau > T_0. \end{cases}$$

We plug this into the slow equations derived from (4.2) to determine the evolution of cell 2.

Cell 2's response depends on several factors, both intrinsic and synaptic. The synaptic factors include

- whether the synapse is excitatory or inhibitory (that is, v_{syn}),
- whether cell 2 is oscillatory for some levels of input,
- the rate at which the synapse turns off (controlled by β),
- the strength of synaptic input (represented by g_{syn}).

Our geometric approach will be very useful in determining how each of these factors influence cell 2's response. This information will then allow us to classify the sorts of waves which emerge in large arrays of cells.

4.3. Response to inhibitory input. Since the analyses in sections 5 and 6 will focus on the effects of inhibitory coupling in networks, we prepare the ground here by discussing how cell 2 may respond to inhibitory input from cell 1. Let $v_{syn} < v$ along singular solutions, which implies that $\mathcal{C}_0$ lies below $\mathcal{C}_1$ for $v > v_{syn}$. There are two main cases to consider, depending on whether $\mathcal{C}_1$ is oscillatory or excitable (recall that $\mathcal{C}_0$ is always taken to be excitable).

First, suppose that $\mathcal{C}_1$ is oscillatory. When cell 1 fires, cell 2 jumps from the rest point on $\mathcal{C}_0$ to the left branch of $\mathcal{C}_1$. If T_0 is sufficiently large, then cell 2 will evolve along the left branch of $\mathcal{C}_1$ all the way to the knee, and then jump up at some time

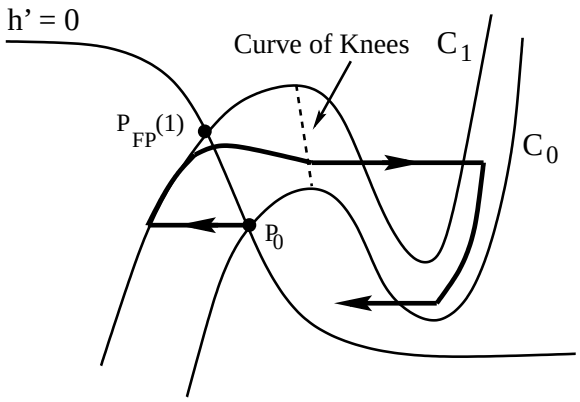

FIG. 6. *PIR. While a cell receives inhibitory input, it evolves along the left branch of C_1. After it is released from inhibition, the cell will jump up to the active phase if it can "escape" by reaching the curve of left knees.*

$T_1 < T_0$. Hence, cell 2 is able to "*escape*" its silent phase by reaching the curve of left knees while cell 1 is still active.

Now let us assume that $\mathcal{C}_1$ is excitable. In this case cell 2 evolves up the left branch of $\mathcal{C}_1$ toward the stable fixed point $P_{FP}(1)$ during $0 < \tau < T_0$, while cell 1 is active. At $\tau = T_0$, cell 1 jumps down and the synaptic variable $s_1(\tau)$ begins to decay. If, at this time, cell 2 lies above the left knee of $\mathcal{C}_0$ and the inhibitory input it receives is decaying relatively fast, then it will fire. This mechanism of firing is referred to as *postinhibitory rebound* (PIR). It is often considered to be a "*release*" phenomenon, whereby the ending of cell 1's active phase removes the inhibition felt by cell 2, thus switching cell 2 from silent to active. We remark, though, that the dynamics of PIR can be much more complex and subtle than the simple description above reveals. If the synaptic activation and deactivation constants were both $O(1)$, then indeed, the release of cell 2 from inhibition would occur instantaneously on the slow time scale, so rebound firing would be elicited immediately. However, if the synaptic decay rate is $\epsilon\beta = O(\epsilon)$, as in our model, then the inhibitory influence will remain even after the active cell stops firing. So whether rebound firing actually occurs will depend on if cell 2 can *escape* the residual inhibition by reaching the curve of knees. In other words, when there are slow synaptic processes at work, PIR is a combination of "release" and "escape" mechanisms; see Figure 6.

The arguments above demonstrate that cell 2 can fire due to PIR if g_{syn}, T_0, and β are all sufficiently large: g_{syn} needs to be large so that $h_{FP}(1) > h_{LK}(0)$, which ensures that if T_0 is big enough, then cell 2 lies above the left knee of $\mathcal{C}_0$ when $\tau = T_0$; we need β to be sufficiently large so that the synaptic input decays rapidly enough for cell 2 to be able to reach the curve of left knees. If β is too small, then cell 2 will follow close to the fixed points $P_{FP}(s_1(\tau))$ and return to rest.

The slow variables governing the behavior of cell 2 are h_2 and s_1. Reduced equations for their evolution can be derived. This slow subsystem cannot typically be solved explicitly since the h_2 equation is in general nonlinear, but it nevertheless provides a helpful way to visualize and interpret solutions. We depict in Figure 7 the projection of cell 2's trajectory onto the (h_2, s_1) slow phase plane. The bold curve represents cell 2's trajectory; it begins at the rest point p_0 and jumps vertically to $\{s_1 \equiv 1\}$ when cell 1 fires. It then moves horizontally toward $(h_{FP}(1), 1)$ until cell 1

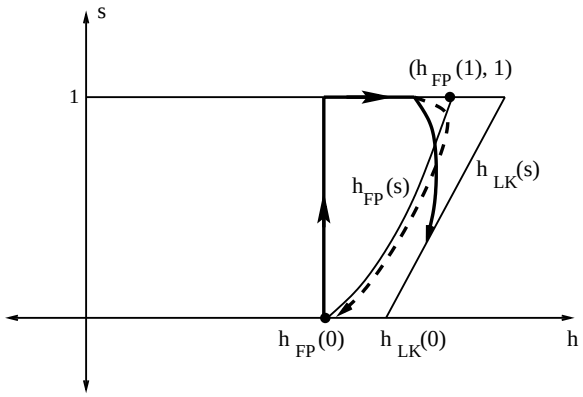

FIG. 7. *Slow phase plane. The slow variables are h and s (subscripts have been dropped). If the trajectory can reach the curve of left knees* $\{h = h_{LK}(s)\}$*, as the bold curve does, then the cell will jump up to the active phase. If the parameter* β *is too small, then this will not be possible, as illustrated by the dashed curve.*

jumps down at time $\tau = T_0$. For $\tau > T_0$, $s_1(\tau)$ decreases. Cell 2 fires if its trajectory is able to reach the curve $\{h = h_{LK}(S)\}$. As discussed earlier, if β is too small, the trajectory will stay close to $\{h = h_{FP}(S)\}$; this is illustrated by the dashed curve in Figure 7.

5. Smooth waves.

5.1. Introduction. Smooth waves arise when cells are able to leave their silent phase without having to wait for presynaptic cells to jump down first. As we have described in the preceding section, a cell could manage this if, while receiving some nontrivial level of inhibitory input S, it lies on a cubic that is oscillatory. However, we mentioned in the introduction that there are other possible mechanisms. In this section, we show that smooth propagation of activity may arise even if each $\mathcal{C}_S$ is excitable, providing the synaptic footprint is off-centered.

Consider a one-dimensional continuous array of cells coupled through mutual inhibition. A smooth wave corresponds to a traveling wave solution of (2.4); that is, it is a solution of (2.4) of the form

$$(v(x,t), h(x,t), s(x,t)) \;=\; (v(\xi), h(\xi), s(\xi)), \qquad \xi \;=\; x + \epsilon ct.$$

Plugging the above into (2.4), we find that (v, h, s) satisfy the system

$$\begin{aligned} \epsilon c v' &= f(v,h) - g_{syn} S_{tot}(\xi)(v - v_{syn}), \\ \epsilon c h' &= \epsilon(h_\infty(v) - h)/\tau_h(v), \\ \epsilon c s' &= \alpha(1-s)H(v-\theta) - \epsilon\beta s, \end{aligned} \tag{5.1}$$

where the derivative is with respect to ξ and

$$S_{tot}(\xi) = \int_{-\infty}^{\infty} W(\xi - y) s(y)\, dy. \tag{5.2}$$

A smooth wave is then a solution of (5.1) that satisfies the boundary conditions

$$(v, h, s)(\pm\infty) \;=\; (v_0, h_0, 0).$$

We will consider $c > 0$, that is, waves moving to the left. Note, also, that the velocity of the wave is taken to be $O(\epsilon)$.

We can reduce this integral-differential equation to a system of ordinary differential equations (ODEs) as follows. Consider a solitary (single-peaked) pulse and assume that $v(\xi) > \theta$ if and only if $0 < \xi < a$, where the constant a is yet to be determined. Once c and a are known, we can solve the third equation in (5.1) for $s(\xi)$. In the limit $\epsilon \to 0$, we find that

$$s(\xi) = \begin{cases} 0 & \text{if } \xi < 0, \\ 1 & \text{if } 0 < \xi < a, \\ \exp\left\{-\frac{\beta}{c}(\xi - a)\right\} & \text{if } \xi > a. \end{cases} \tag{5.3}$$

Now plug this formula for $s(\xi)$ into (5.2) to obtain an expression for $S_{tot}(\xi)$. Since this depends on the unknown constants c and a, we will sometimes write $S_{tot}(\xi; c, a)$. The first two equations in (5.1) can then be treated as a system of nonautonomous ODEs.

5.2. The singular trajectory. As described in section 4, we construct a singular solution of (5.1) by dissecting the trajectory into different pieces corresponding to either the silent or active phases or to a transition between these phases. Over each piece, the solution satisfies reduced equations in either the fast or slow variables. We begin our construction at $\xi = -\infty$ and increase ξ, describing the singular trajectory in the (v, h) phase plane along the way.

We will assume a footprint of unit length; that is, $W(\xi) = 0$ for $|\xi| \geq 1$. The translation of the wave is chosen so that the initial jump up to the active phase occurs at $\xi = 0$. It then follows that for $\xi < -1$, we have $S_{tot}(\xi) = 0$, and $(v(\xi), h(\xi))$ lies at the rest point (v_0, h_0) on the left branch of the $S_{tot} = 0$ cubic.

For $-1 < \xi < 0$, the cells lie in the silent phase along the left branch of the cubic associated with $S_{tot}(\xi)$, which we write as $v = v_L(h, S_{tot})(\xi)$. The variable $h(\xi)$ evolves according to the second equation in (5.1), a nonautonomous ODE in which $v = v_L(h, S_{tot})(\xi)$. We view $h(\xi)$ and $S_{tot}(\xi)$ as the slow variables. Note that they depend on the unknown constants a and c. These constants should be chosen so that $(h(0), S_{tot}(0))$ lies on the curve of knees $h = h_{LK}(S)$ in the slow phase plane (since the jump-up to the active phase is supposed to occur at $\xi = 0$). Such a choice may not be possible, in which case the smooth wave will not exist.

For example, take a square on-center synaptic footprint, without gaps. In this case, $S_{tot}(\xi)$ is nearly constant while in the silent phase; so, given that the cells are excitable for all levels of synaptic input, $(v(\xi), h(\xi))$ must approach the fixed point along the left branch of the cubic associated with this constant S_{tot} level. A smooth wave is therefore not possible. In contrast, if there is a gap in the synaptic footprint, then $S_{tot}(\xi)$ will achieve a maximum at some point $\xi_0 \in (-1, 0)$ and then begin to decrease. For simplicity of calculation, we work with a synaptic footprint of unit length that has rectangular peaks and a gap of length 2γ between them, as described in the appendix. We see that S_{tot} reaches a maximum at $\xi = -\gamma$, after which it decreases as $\xi \to 0$. In this case $(h(\xi), S_{tot}(\xi))$ is able to evolve to the curve of knees, thus escaping the silent phase and making possible the existence of a smooth wave. We will denote the jump-up point on the curve of knees by (h_J, S_J).

A reduced equation for the fast jump up can be derived by introducing the fast variable $\eta = \xi/\epsilon$ into the first two equations of (5.1) and then letting $\epsilon = 0$. This yields the fast equations $cv' = f(v, h) - g_{syn} S_{tot}(0)(v - v_{syn})$ and $h' = 0$, where

differentiation is now with respect to η. Along the jump up, both h and S_{tot} are constant; that is, $(h, S_{tot}) = (h_J, S_J)$. During the active phase, when $0 < \xi < a$, $(v(\xi), h(\xi))$ travels along the right branch of the cubic determined by $S_{tot}(\xi)$. There is then a jump down at $\xi = a$. As with the jump up, we can obtain a reduced equation for v with both h and S_{tot} constant. This is as far as we'll take the description of the singular solution for now.

5.3. Estimating the wave speed. The singular construction allows us to obtain estimates on the wave speed. This is based on reducing the integral-differential system (5.1) to a two-point boundary value problem involving the unknown parameters a and c. The boundary value problem can then be solved using the numerical continuation package AUTO [6].

Consider (5.1) for $-1 \le \xi \le 0$; recall that this corresponds to the silent phase of the singular solution. We begin by writing the first two equations of (5.1) as the autonomous system

$$\begin{aligned} \epsilon c v' &= f(v,h) - g_{syn} S_{tot}(x)(v - v_{syn}), \\ c h' &= (h_\infty(v) - h)/\tau_h(v), \\ x' &= 1. \end{aligned} \tag{5.4}$$

Note that there are three dependent variables along with two unknown parameters a and c. In order to have a unique solution, we need to specify boundary conditions.

Since, as stated in section 5.2, $(v(\xi), h(\xi)) = (v_0, h_0)$ for $\xi < -1$, a natural condition at $\xi = -1$ is

$$v(-1) = v_0, \quad h(-1) = h_0, \quad \text{and} \quad x(-1) = -1. \tag{5.5}$$

For a boundary condition at $\xi = 0$, we use the fact that this is when the jump up takes place, and that $(v(0), h(0))$ must lie on the curve of left knees. We assume that this curve is linear, i.e., $h_{LK}(S) = h_{LK}(0) + \lambda S$ for some constant λ whose value can be estimated from plots of nullclines. Hence, we have the boundary condition

$$h(0) = h_{LK}(0) + \lambda S_{tot}(0; c, a), \tag{5.6}$$

where $S_{tot}(0; c, a)$ is calculated from (5.3) and (5.2); see, for example, the formula shown in the appendix.

To complete the system, one more condition relating the parameters is needed. This arises by considering the active phase of the singular solution. During the active phase, when $0 < \xi < a$, reasonable simplifying assumptions are that $h_\infty(v) = 0$ and $\tau(v) = \tau_R$ for some positive constant τ_R. These imply that $h(\xi)$ satisfies $ch' = -h/\tau_R$, and hence $h(\xi) = h(0)e^{-\xi/c\tau_R}$. We will further assume that $S_{tot} = 0$ at the jump down. This is not quite correct; however, provided β is not too small, it will be a reasonable approximation as numerical simulations will show. It then follows that $h_{RK}(0) = h(0)e^{-a/c\tau_R}$, or

$$a = c\tau_R \ln\left(\frac{h(0)}{h_{RK}(0)}\right) = c\tau_R \ln\left(\frac{h_{LK}(0) + \lambda S_{tot}(0)}{h_{RK}(0)}\right). \tag{5.7}$$

Note that $S_{tot}(0)$ depends on a so this is a nonlinear implicitly defined condition on a. Our boundary value problem therefore consists of the ODEs (5.4) together with the boundary conditions (5.5), (5.6), and (5.7). There are five conditions for this

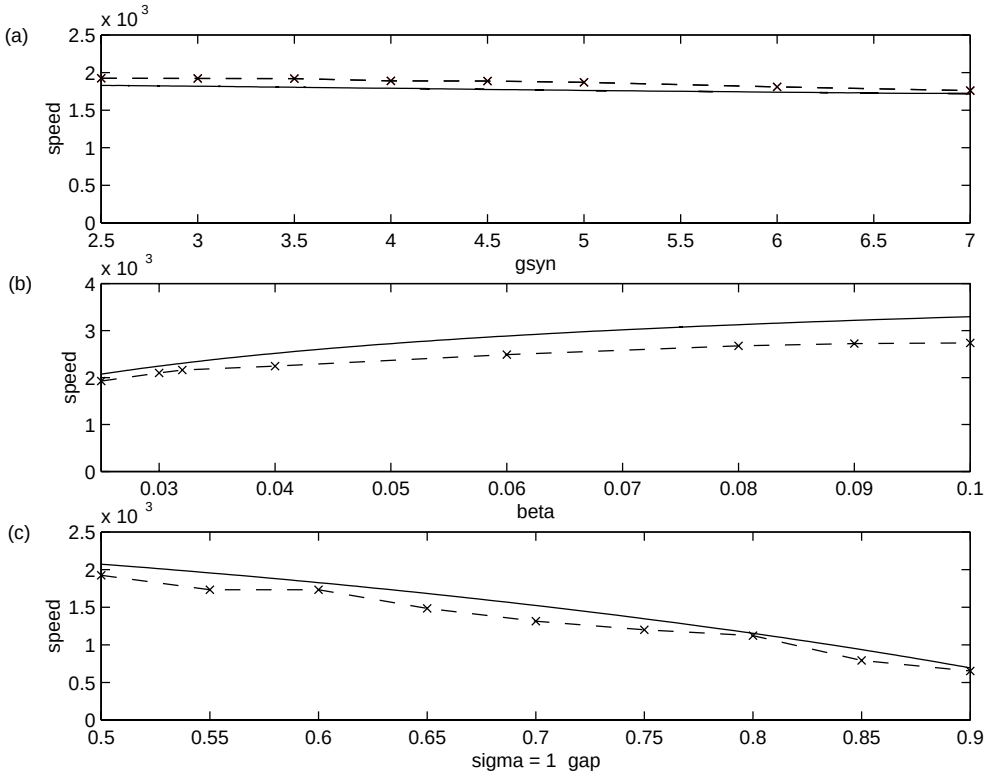

FIG. 8. *Plots of wave speed versus parameters for smooth waves:* (a) g_{syn}*;* (b) β*;* (c) $\sigma \equiv 1-\gamma$*, where* γ *is the gap size of the synaptic footprint. The solid curves were obtained from the two-point boundary value problem, and the dashed curves directly from the integral-differential equations. The parameter ranges shown are those for which a pulse can be found in both of the systems. In each plot, the nonvarying parameters are set at their default (or "starting") values given in the appendix.*

three-dimensional system. However, we have two free parameters, the pulse width, a, and the velocity, c, so there is a possibility for finding solutions.

Results obtained from using AUTO are shown in Figures 8 and 9. The solid curves were obtained from the two-point boundary value problem described here, while the dashed curves were computed by first numerically solving the integral-differential equations of (2.4) and then measuring the velocity of the resulting smooth wave. Observe that the speed varies noticeably with respect to β, τ_R and the gap size of the synaptic footprint; it does not depend much on g_{syn}, a parameter that manifests itself in the strength of inhibition between cells, nor on τ_L, which measures the rate of recovery of each cell while in its silent phase.

In Figure 10(a), we plot the v-component of a single-pulsed solution to (5.1) against position x at a fixed time, and show also the solution of the two-point boundary value problem. In Figure 10(b) we plot S_{tot}, and in Figure 10(c) the h-component is plotted. Note that S_{tot} decreases sharply just before the cell fires. It is during this period that a gap in the inhibitory input to cells allows them to reach the curve of knees and "escape." In Figure 10(d), we plot the projection of $(v(\xi), h(\xi))$ onto the (v, h) phase plane and in Figure 11, we show the projection of $(h(\xi), S_{tot}(\xi))$ onto the phase plane of slow variables. Our numerics demonstrate that the solution of (5.1) behaves closely to that predicted by the singular perturbation construction. In

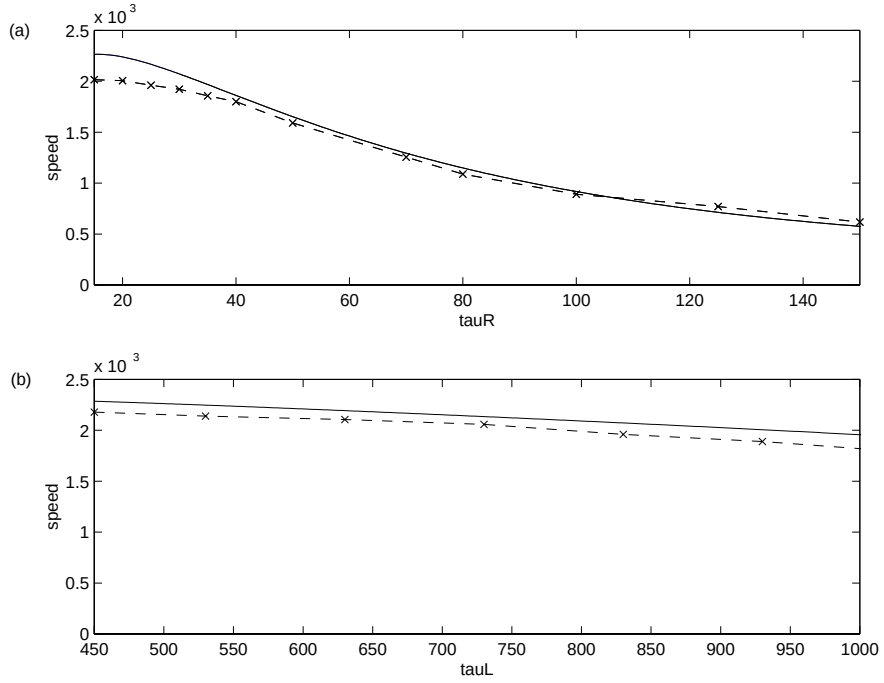

FIG. 9. *Plots of wave speed versus* (a) τ_R *and* (b) τ_L *for smooth waves. See caption of Figure* 8 *for more explanation.*

particular, the trajectories follow the nullcline determined by $S_{tot}(\xi)$; moreover, the jumps up and down occur at left and right knees. Views of a two-pulsed solution, found at small values of the gap size, are shown in Figure 12.

5.4. A priori estimates on the wave speed and gap size. In this subsection we demonstrate how one can derive analytical estimates on the wave speed. We also present estimates on how large the gap in the synaptic footprint should be for there to exist a singular smooth wave. Our calculations here are done using the rectangular-peaked footprint described in section 5.2 and in the appendix, and cells are assumed to be excitable for all levels of synaptic input. First, we need the following lemmas.

LEMMA 5.1. *Let a be the width of the singular smooth pulse; then* $0 < a < 1$.

Proof. If $a \geq 1$, then $S_{tot}(\xi) = 1/2$ for $-\gamma \leq \xi \leq 0$. That is, $(v(\xi), h(\xi))$ lies on the left branch of the $S_{tot} = 1/2$ cubic for $-\gamma \leq \xi \leq 0$. It is then impossible for (v, h) to lie along the curve of knees at $\xi = 0$ in order to jump up to the active phase. Hence, a smooth wave cannot exist. ∎

LEMMA 5.2. *There exists $\delta_0 > 0$, that does not depend on γ, such that $S_{tot}(-\gamma) - S_{tot}(0) > \delta_0$.*

Proof. Note that the curves $h_{FP}(S)$ and $h_{LK}(S)$ are monotone increasing. Let $S_{FP}(h)$ and $S_{LK}(h)$ denote their inverses, respectively. The assumption that each cell is excitable for fixed levels of input implies that there exists $\delta_0 > 0$ such that $S_{FP}(h) - S_{LK}(h) > \delta_0$ for each h for which both curves are defined.

Now $(h(\xi), S_{tot}(\xi))$ reaches a maximum value of S_{tot} at $\xi = -\gamma$ and then must cross the fixed point curve at some $\xi_0 \in (-\gamma, 0)$ before it can jump up. It follows that

$$S_{tot}(-\gamma) > S_{tot}(\xi_0) \;=\; S_{FP}(h(\xi_0)). \tag{5.8}$$

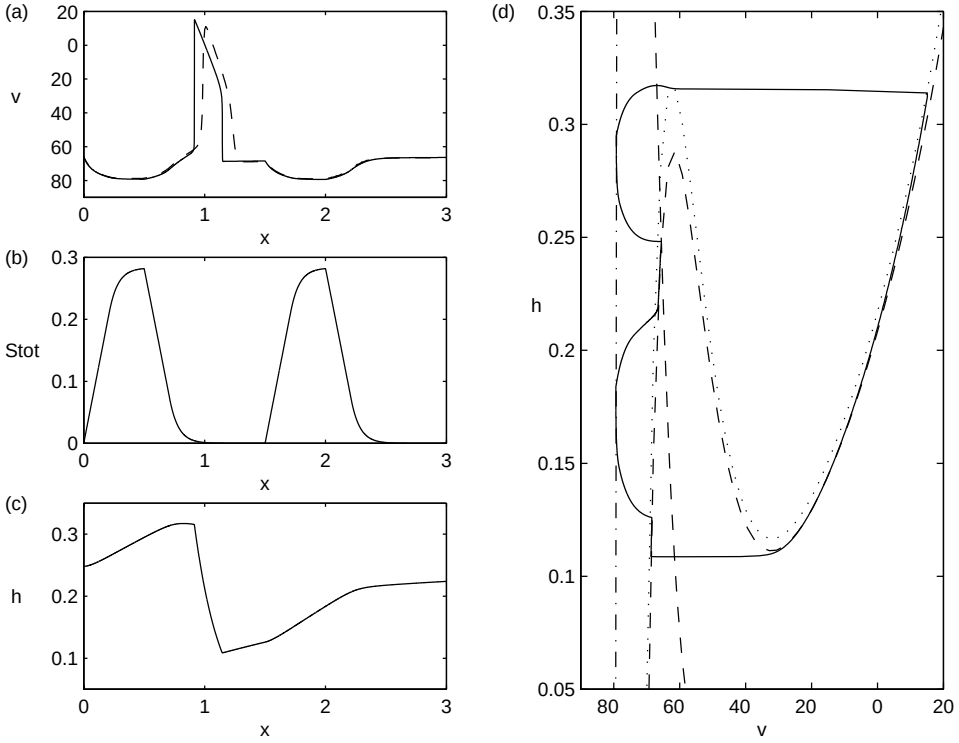

FIG. 10. *Various perspectives of the one-pulsed solution:* (a) *Plot of v versus x; the solid curve was obtained from the two-point boundary value problem, and the dashed curve from the integral-differential system, at a fixed time t.* (b) *Plot of S_{tot} versus x.* (c) *Plot of h versus x.* (d) *Projection of solution trajectory (solid curve) onto the (v,h) phase plane; the dashed curves are the nullclines for $S_{tot} = 0$, the dotted curve is the cubic-shaped nullcline for $S_{tot} \approx 0.0055$, and the dot-dashed curve corresponds to the cubic-shaped nullcline for $S_{tot} \approx 0.28$.*

Moreover, $h'(\xi) < 0$ for $\xi \in (\xi_0, 0)$, and hence $h(\xi_0) > h(0)$. Since $S_{LK}(h)$ is monotone increasing, it follows that

$$S_{LK}(h(\xi_0)) > S_{LK}(h(0)) \;=\; S_{tot}(0). \tag{5.9}$$

The last equality holds because the jump-up is at $\xi = 0$. From (5.8), (5.9), and the definition of δ_0, we conclude that

$$S_{tot}(-\gamma) - S_{tot}(0) \;>\; S_{FP}(h(\xi_0)) - S_{LK}(h(\xi_0)) \;>\; \delta_0,$$

as claimed. □

To derive a priori bounds on the wave speed, we obtain from (5.7) and Lemma 5.1 the upper bound

$$c \;=\; a\left\{\tau_R \ln\frac{h(0)}{h_{RK}(0)}\right\}^{-1} \;<\; \left\{\tau_R \ln\frac{h_{LK}(0)}{h_{RK}(0)}\right\}^{-1}.$$

In order to obtain a lower bound, we can calculate that if $a < 1 - \gamma$, then

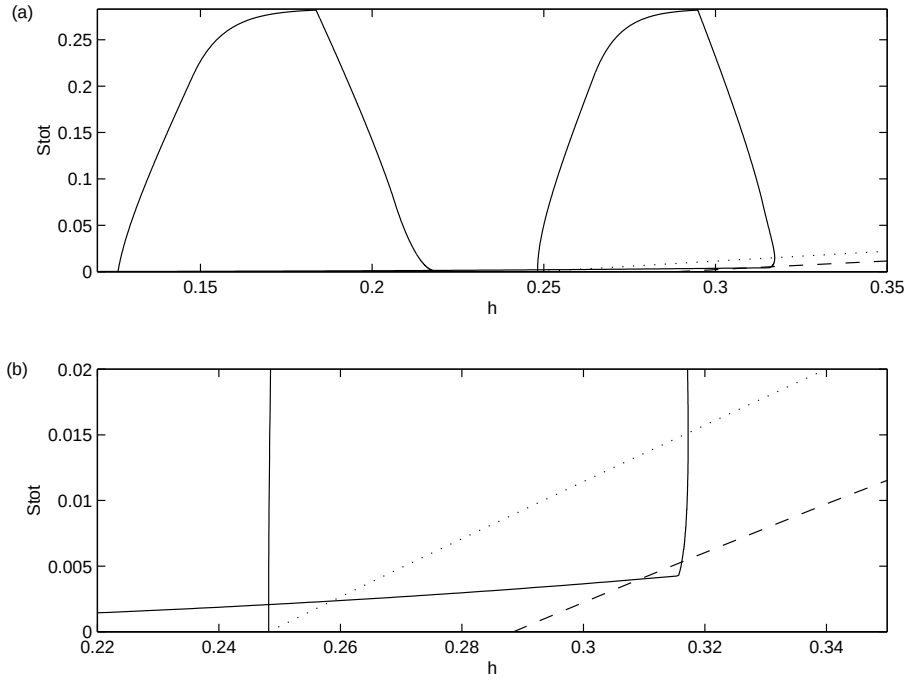

FIG. 11. *Plots of the solution trajectory (solid curve) corresponding to the smooth wave in the phase plane of slow variables h and S_{tot}.* (b) *zooms in on a portion of* (a). *The dashed curve is the curve of left knees $\{h = h_{LK}(S_{tot})\}$; the dotted curve is the curve of fixed points $\{h = h_{FP}(S_{tot})\}$.*

$$\begin{aligned} S_{tot}(-\gamma) &= \frac{1}{2(1-\gamma)}\left(\frac{c}{\beta}(1-e^{\frac{\beta}{c}(\gamma+a-1)})+a\right) \\ &< \frac{1}{2(1-\gamma)}\left(\frac{c}{\beta}+a\right) \;=\; \frac{c}{2(1-\gamma)}\left(\frac{1}{\beta}+\tau_R \ln\frac{h_J}{h_{RK}(0)}\right) \\ &< \frac{c}{2(1-\gamma)}\left(\frac{1}{\beta}+\tau_R \ln\frac{1}{h_{RK}(0)}\right). \end{aligned}$$

Together with Lemma 5.2, this implies that

$$c \;>\; 2\delta_0(1-\gamma)\left(\frac{1}{\beta}+\tau_R \ln\frac{1}{h_{RK}(0)}\right)^{-1}.$$

If $a \geq 1-\gamma$, then a lower bound for c follows from (5.7).

Next, we find a lower bound on the gap size. First we assume that $\gamma < \min\{a, (1-a)\}$; then using Lemma 5.2 and the formula for S_{tot} in the appendix, we find that

$$\delta_0 < S_{tot}(-\gamma) - S_{tot}(0) = \frac{1}{2(1-\gamma)}\left\{\frac{c}{\beta}\left(e^{\frac{\beta}{c}(a-1)} - e^{\frac{\beta}{c}(\gamma+a-1)}\right)+\gamma\right\} < \frac{\gamma}{2(1-\gamma)},$$

and hence $\gamma > \frac{2\delta_0}{1+2\delta_0}$. A similar analysis holds if either $\gamma > a$ or $\gamma > 1-a$, with help from the bounds on c.

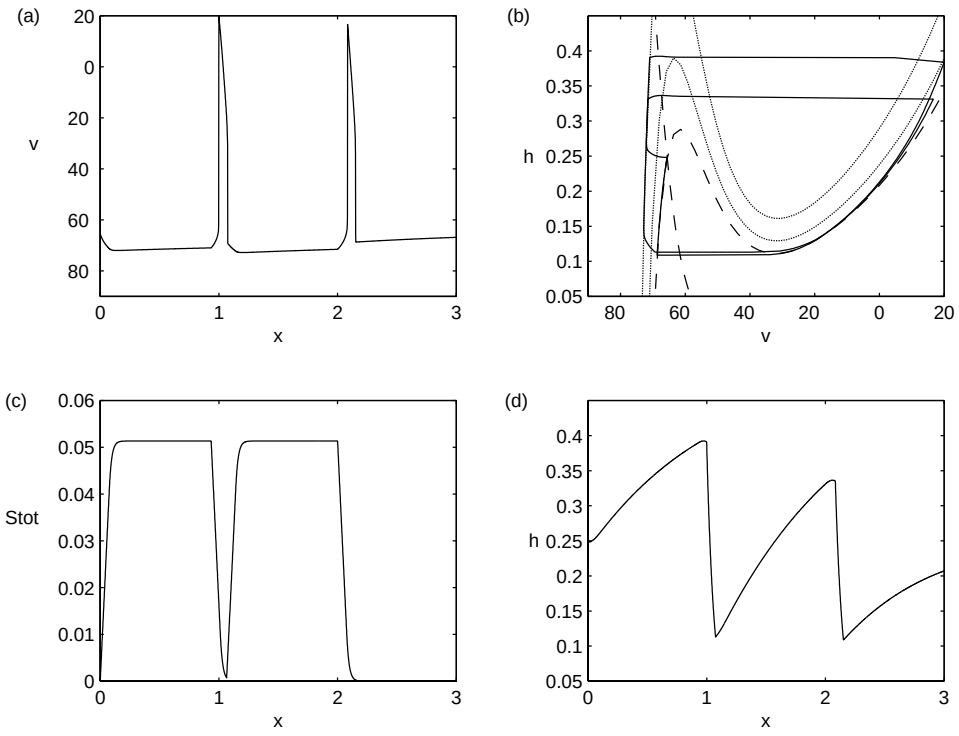

FIG. 12. *Various perspectives of a two-pulsed solution, which was found for* $\gamma \approx 0.1$ *(in general, multipeaked waves can be generated at small values of* γ*):* (a) *Plot of* v *versus* x. (b) *Projection of solution trajectory (double-looped solid curve) onto the* (v, h) *phase plane; the dashed curves are the nullclines for* $S_{tot} = 0$*, the dotted curve is the cubic-shaped nullcline for* $S_{tot} \approx 0.0186$*, and the dot-dashed curve corresponds to the cubic-shaped nullcline for* $S_{tot} \approx 0.0515$. (c) *Plot of* S_{tot} *versus* x. (d) *Plot of* h *versus* x.

6. Lurching waves.

6.1. Introduction. We view lurching waves as activity propagating through a network of cells via post inhibitory rebound. As in section 5, consider a one-dimensional continuous array of cells coupled with synaptic inhibition. We begin with every cell at rest and excite a certain group of cells in the array, inducing them to fire. This group of active cells will inhibit a cluster of cells ahead of it, and the inhibited cells may then fire due to PIR after the active group returns to the silent phase. If this process continues along the array, a lurching wave is produced. Consecutive leading active clusters need not be adjacent to each other (see [12]), although this is the case for each example shown in Figure 5.

Recall from section 5 that a smooth wave cannot exist if the cells are excitable for all levels of inhibitory input and the synaptic footprint is on-centered. In this section we shall show that, in contrast, a lurching wave can be constructed under these conditions. Note, however, that we do not preclude the possibility of lurching waves existing when the connectivity is off-centered. Indeed, analysis for the off-centered case will be very similar to that presented in the following subsection, leading to slightly different formulas, as mentioned in the appendix.

6.2. Analysis of solitary lurching pulses. Here we present the singular construction of a solitary lurching pulse like the one illustrated in Figure 5(a). To simplify the calculations, we will make a number of assumptions. Comparisons of how well our formulas predict the velocity of lurching waves in network simulations are given at the end of this section.

First, we suppose that consecutive active clusters are adjacent to each other and of the same size. Let us denote the size of each cluster by ϕ; in other words, ϕ will be the width of our lurching pulse. This width is not known a priori, but an implicit formula will be derived for it in subsection 6.4. We further assume that all cells within the same cluster receive the same amount of total synaptic inhibition. This implies that cells belonging to the same cluster are completely synchronized with each other, which allows us to view them as lying along a single trajectory in phase space. We remark that even if the total synaptic input within each cluster is not constant, cells within each cluster will typically still be nearly synchronized. The geometric approach can then be used to obtain bounds on the wave speed. We shall work with a square, on-centered, synaptic footprint: $W(x) = 1$ for $|x| < \sigma$, and $W(x) = 0$ otherwise.

Suppose that at time $\tau = 0$, the active cluster consists of those cells with position $x \in (-\phi, 0)$. Let us call this cluster G_1. When G_1 falls down to the silent phase, cells with $0 < x < \phi$ jump up to form the new active cluster. This new cluster will be denoted G_2, and the time at which G_2 jumps up will be called T_{tot}. We shall derive a formula for T_{tot}. The velocity of the lurching pulse can then be computed in terms of ϕ and T_{tot}.

Next, we calculate the total synaptic input to each cell. Assume that the synapses turn off quickly (on the slow $\tau = \epsilon t$ time scale), i.e., β is large. It then follows that, in the singular limit $\epsilon \to 0$, each $s(x,\tau) = 1$ whenever $v(x,\tau) > \theta$, and $s(x,\tau) = 0$ otherwise. Since the cells within G_1 are active for $0 < \tau < T_{tot}$, it follows that if $0 < \tau < T_{tot}$, then $s(x,\tau) = 1$ for $-\phi < x < 0$, and $s(x,\tau) \approx 0$ for other x. Note that if $\sigma > 2\phi$, then $S_{tot}(x,\tau) = \int_{-\infty}^{\infty} W(x-y)s(y,\tau)\,dy \approx \phi$ whenever $|x| < \phi$ and $0 < \tau < T_{tot}$; that is, the total synaptic input felt by cells within both the G_1 and G_2 clusters is approximately at the same level, namely, ϕ, as long as G_1 is active. A similar analysis shows that, in the case of a solitary pulse, this also holds when G_2 is active. We remark that if there is further activity in the wake of the wave, more complicated interactions may occur, so throughout this section we focus on solitary lurching waves. In the next subsection, conditions on parameters will be derived to ensure that cells fire only once as the wavefront passes; that is, the network returns to silence in the wake of the wave. As pointed out above, even if the condition $\sigma > 2\phi$ is not satisfied, cells within each cluster will be almost synchronized and the geometric methods can then be used to obtain a priori bounds on the wave speed. This is discussed further at the end of section 6.4.

We denote the trajectory of cells within G_1 as $(v_1(\tau), h_1(\tau), s_1(\tau))$ and the trajectory of cells within G_2 as $(v_2(\tau), h_2(\tau), s_2(\tau))$. These trajectories are illustrated in Figure 13. At $\tau = 0$, G_1 lies along the curve of knees, poised to jump up to the active phase. G_2 lies at the rest point p_0 and jumps to the left branch of $\mathcal{C}_\phi$. For $\tau > 0$, G_1 moves down the right branch of $\mathcal{C}_\phi$ and G_2 moves up the left branch of $\mathcal{C}_\phi$. This continues until G_1 reaches the right knee of $\mathcal{C}_\phi$ and jumps down. Suppose that this happens at time T_A. Then the synaptic variable $s_1(\tau)$ begins to decrease and release G_2 from inhibition. The cycle is complete when G_2 reaches the curve of knees, which we assume is at $\tau = T_{tot}$. In order to be a lurching pulse, we require that the position of G_2 at $\tau = T_{tot}$ is precisely the same as the initial position of G_1 at $\tau = 0$. This will

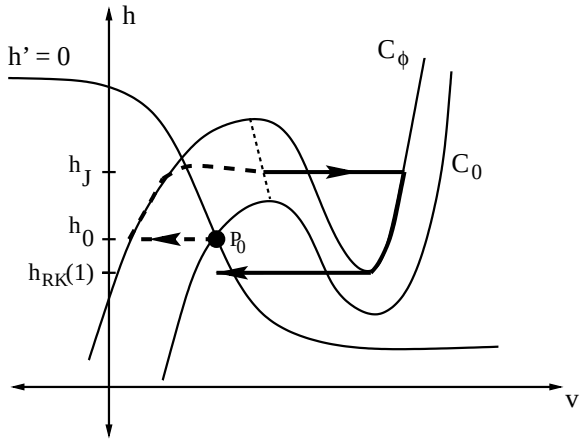

FIG. 13. *Singular solutions corresponding to a lurching wave. The solid curve is the trajectory of G_1, while the dashed curve represents the trajectory of G_2.*

lead to an analytic expression for T_{tot}.

We now list some simplifying assumptions concerning the nonlinear functions in the model. All of these assumptions are nearly satisfied for the system given in the appendix, and numerical simulations demonstrate that they lead to accurate expressions for the wave speed.

(A1) In the silent phase, $\tau(v) = \tau_L$, a constant.
(A2) In the active phase, $\tau(v) = \tau_R$, a constant, and $h_\infty(v) = 0$.
(A3) The left branches $v = v_L(h, S)$ of $\mathcal{C}_S$ do not depend on h.
(A4) The curve of left knees is linear: there exists λ such that $h_{LK}(S) = h_{LK}(0) + \lambda S$. In the models we consider, λ is positive.

To explain (A3), note that the cubic $\mathcal{C}_S$ is given by $g_L(v - v_L) + g_{Ca}m_\infty(v)h(v - v_{Ca}) + g_{syn}S(v - v_{syn}) = 0$ and in the silent phase, $m_\infty(v)$ is very small. So if we take $m_\infty(v) = 0$ in the silent phase, then the left branch of $\mathcal{C}_S$ is given by

$$v = \frac{g_L v_L + g_{syn} v_{syn} S}{g_L + g_{syn} S}.$$

Observe that under (A2), equation (4.1), which describes the evolution of $h(\tau)$ in the active phase, simplifies to

$$\dot{h} = -h/\tau_R \,. \tag{6.1}$$

From (A1) we obtain that in the silent phase, $h(\tau)$ satisfies the equation

$$\dot{h} = (h_\infty(v) - h)/\tau_L \,. \tag{6.2}$$

Using (A3), we see that on the left branch of $\mathcal{C}_S$ for any fixed S, v takes a constant value, which must then be $v_{FP}(S)$; therefore, $h_\infty(v)$ is also a constant, namely, $h_{FP}(S)$, and hence we have the following equation describing behavior in the silent phase:

$$\dot{h} = (h_{FP}(S) - h)/\tau_L \,. \tag{6.3}$$

We now consider T_A. Suppose that G_1 jumps up at $h_1 = h_J$, where h_J is yet to be determined. It then follows from (A2) that for $0 < \tau < T_A$, $h_1(\tau)$ satisfies (6.1)

subject to $h_1(0) = h_J$. Now G_1 jumps down at the right knee of $\mathcal{C}_\phi$ at $\tau = T_A$. This implies that $h_1(T_A) = h_{RK}(\phi)$. Solving (6.1) together with these two boundary conditions leads to the following expression relating the unknowns h_J and T_A:

$$T_A = \tau_R \ln \frac{h_J}{h_{RK}(\phi)}. \tag{6.4}$$

We next compute an expression for $T_S \equiv T_{tot} - T_A$. This is the time from when G_1 jumps down until G_2 reaches the curve of left knees and jumps up. For $T_A < \tau < T_{tot}$, $s_1(\tau)$ satisfies $\dot{s_1} = -\beta s_1$ with $s_1(T_A) = 1$. Hence, $s_1(\tau) = e^{-\beta(\tau - T_A)}$ and therefore

$$S_{tot}(x,\tau) = \int_{-\infty}^{\infty} W(x-y)s_1(\tau)dy = \phi e^{-\beta(\tau - T_A)} \quad \text{for} \quad |x| < \phi. \tag{6.5}$$

Since G_2 jumps up at $\tau = T_{tot}$, it must lie at the left knee of the cubic determined by $S_{tot}(T_{tot})$. That is, $h_2(T_{tot}) = h_{LK}(S_{tot}(T_{tot}))$. From (A4) and (6.5), this implies that

$$h_2(T_{tot}) = h_{LK}(0) + \lambda\phi e^{-\beta(T_{tot} - T_A)}.$$

Now the position of G_2 at T_{tot} should be the same as the position of G_1 at $\tau = 0$. In particular $h_2(T_{tot}) = h_1(0) = h_J$. Since $T_S = T_{tot} - T_A$, we conclude that

$$T_S = \frac{1}{\beta} \ln \frac{\lambda\phi}{h_J - h_{LK}(0)}. \tag{6.6}$$

Now (6.4) and (6.6) give two equations for the three unknowns T_S, T_A, and h_J. We obtain a third equation by explicitly solving for $h_2(T_{tot})$. This is done as follows.

In the silent phase, $h_2(\tau)$ follows the left branch of $\mathcal{C}_\phi$ for $0 < \tau < T_A$, and therefore satisfies (6.3) with $S \equiv \phi$ and the initial condition $h(0) = h_0$, where h_0 corresponds to the rest point on $\mathcal{C}_0$. Hence,

$$h_2(\tau) = h_{FP}(\phi) + (h_0 - h_{FP}(\phi))e^{-\tau/\tau_L}. \tag{6.7}$$

To simplify the calculations, we continue to assume that β is rather large. This implies that G_2 moves nearly horizontally from the left branch of $\mathcal{C}_\phi$ to the curve of knees as shown in Figure 13. In other words, we assume that during this transition, i.e., for $T_A < \tau < T_{tot}$, we have $h_2(\tau) \equiv h_2(T_A)$. In particular, $h_2(T_A) = h_2(T_{tot}) = h_J$, and we conclude that

$$h_J = h_{FP}(\phi) + (h_0 - h_{FP}(\phi))e^{-T_A/\tau_L}.$$

Together with (6.4) this leads to the relation

$$A_1(h_J) \equiv \frac{h_{FP}(\phi) - h_J}{h_{FP}(\phi) - h_0} = \left(\frac{h_{RK}(\phi)}{h_J}\right)^{\frac{\tau_R}{\tau_L}} \equiv A_2(h_J). \tag{6.8}$$

This is a single equation for the unknown h_J. The other parameters in this equation can be determined (numerically) by properties of a single cell with constant input. Once we solve for h_J, we can compute T_A and T_S from (6.4) and (6.6) and then compute the total duration of one cycle $T_{tot} = T_A + T_S$.

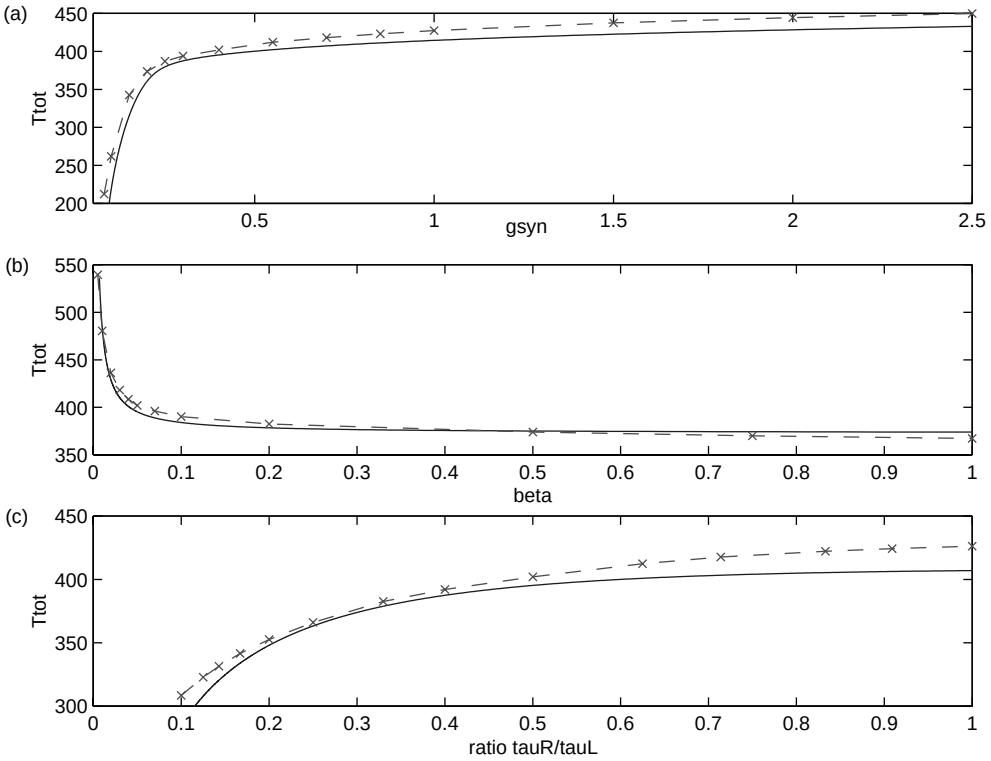

FIG. 14. *Plots of T_{tot} versus parameters for lurching waves:* (a) g_{syn}, (b) β, *and* (c) *the ratio between τ_R and τ_L (active and silent phase rate constants, respectively). The solid curves come from the analytic formulas, and the dashed curves from numerical integration of the discrete network equations. In each plot, the nonvarying parameters are set at their default (or "starting") values given in the appendix.*

This equation has either two roots or no roots. To see this, note that $A_1(0) < \infty$ while $A_2(h)$ approaches ∞ as $h \to 0$. Furthermore, $A_1(h_{FP}(\phi)) = 0 < A_2(h_{FP}(\phi))$. Thus if there is one nontangent root, then there must be another. One of these is close to 0 and the other is close to $h_{FP}(\phi)$, and as the ratio τ_R/τ_L increases, the second root approaches $h_{FP}(\phi)$. Since no jump to the right branch can occur if $h_{FP}(\phi) < h_{LK}(0)$, we see that if we choose the larger root of (6.8), then (6.6) will be defined.

With help from AUTO [6], we computed how T_{tot} changes with respect to various parameters and the results are shown in Figure 14. We picked the larger root of (6.8). The solid curves in Figure 14 represent the solutions of the analytic formulas presented above, while the dashed curves were determined by first numerically integrating the differential equations (2.3) for a discrete array of cells and then measuring the duration of one cycle. Note that a lurching wave does not exist if g_{syn} is too small. In this case, the point $P_{FP}(\phi)$ along $\mathcal{C}_\phi$ might lie below the left knee of $\mathcal{C}_0$ so cells will not be able to jump up to the active phase. As shown in Figure 14(c), lurching waves do not exist if the ratio τ_R/τ_L is too small, that is, if the active phase of each cell is relatively short. This also follows from (6.8). Since $h_0 < h_J < h_{FP}(\phi)$ must hold if h_J exists, the left-hand side of (6.8) must be less than and bounded away from 1. However, if τ_R/τ_L becomes very small, then the right-hand side of (6.8) gets close to 1, and so the equality cannot be satisfied. Finally, recall that in the derivation of

(6.8), we assumed that β is rather large. Figure 14(b) demonstrates that (6.8), (6.4), and (6.6) give an excellent prediction of the wave speed even for small β. Note also that as β increases, T_S decreases and thus T_{tot} approaches the value of T_A, which is independent of β.

6.3. Wake of the wave. Here we derive an analytic condition for when the network returns to rest in the wake of the wave. To determine whether or not cells continue to oscillate, we continue the analysis begun in the preceding subsection. That is, we assume that G_1 fires at $\tau = 0$ and returns to the silent phase at $\tau = T_A$. Moreover, G_2 fires at $\tau = T_{tot} = T_A + T_S$. We ask whether G_1 fires again for some $\tau > T_{tot}$.

As before, we assume β is large, so that the synapses turn off quickly on the $\tau = \epsilon t$ time scale. In this case G_2 jumps up quickly after G_1 returns to the silent phase and releases G_1 from inhibition. In the limit of large β, we have that $T_S = 0$ and $T_{tot} = T_A$. We use these in the arguments that come next. It is clear that the analysis extends to more general cases; however, the resulting formulas are quite a bit more complicated.

Now G_2 lies in the active phase for $T_A < \tau < 2T_A$, during which time G_1 lies in the silent phase along the left branch of $\mathcal{C}_\phi$. At $\tau = 2T_A$, G_2 jumps down and releases G_1 from inhibition. Since the synaptic turn off is fast, G_1 will jump to one of the branches of $\mathcal{C}_0$. If, at this time, G_1 lies below the left knee of $\mathcal{C}_0$, then it will not be able to jump up to the active phase. Hence, a solitary pulse will arise if

$$h_1(2T_A) < h_{LK}(0). \tag{6.9}$$

We derive an analytic expression for this in terms of the network parameters as follows. For $T_A < \tau < 2T_A$, G_1 lies on the left branch of $\mathcal{C}_\phi$ so $h_1(\tau)$ satisfies (6.3) with $S \equiv \phi$. Since G_1 jumps down at $\tau = T_A$, we have that $h_1(T_A) = h_{RK}(\phi)$. Hence, for $T_A < \tau < 2T_A$, $h_1(\tau) = h_{FP}(\phi) + (h_{RK}(\phi) - h_{FP}(\phi))e^{-(\tau - T_A)/\tau_L}$. Therefore,

$$h_1(2T_A) = h_{FP}(\phi) + (h_{RK}(\phi) - h_{FP}(\phi))e^{-T_A/\tau_L}.$$

From (6.4) it follows that (6.9) is satisfied if

$$\frac{h_{FP}(\phi) - h_{RK}(\phi)}{h_{FP}(\phi) - h_{LK}(0)} > \left(\frac{h_J}{h_{RK}(\phi)}\right)^{\tau_R/\tau_L}. \tag{6.10}$$

6.4. The pulse-width. Here we derive an approximation for the width of the pulse. As before, we suppose a group of cells of size ϕ jumps across to the right branch at $\tau = 0$. Cells ahead of the pulse will move up the left branch corresponding to the synaptic input they receive. The active group will move down the right branch of the nullcline until they encounter a right knee and then make the jump back to the left branch. This will release those cells along the left branch that lie above $h_{LK}(0)$. The size of this group of cells must be precisely ϕ. Thus, we will be able to compute a self-consistent equation for the pulse-width ϕ.

We continue to assume that the time each cell spends in the active phase is some constant, T_A, say. It is not necessary to assume, however, that the total synaptic input to cells within each cluster is constant. Note that T_A should, in fact, depend on the amount of synaptic input the cell receives. Later we discuss how one can obtain bounds on this time; this will lead to bounds on the pulse width. We also assume, as before, that the parameter β is large. It then follows that each $s(x, \tau) = 1$ whenever $v(x, \tau) > \theta$ and $s(x, \tau) \approx 0$ whenever $v(x, \tau) < \theta$.

Consider a rightward-moving wave and suppose that when $\tau = 0$, the cells with position $y \in (-\phi, 0)$ are active. Then the total input to the cell at position $x > 0$ is

$$s_{tot}(\phi, x) = \int_{-\phi}^{0} W(x - y)\, dy.$$

The cells ahead of the pulse will evolve along the left branch of the cubic determined by $s_{tot}(\phi, x)$ for time T_A. Let $\hat{h}_{FP}(\phi, x) \equiv h_{FP}(s_{tot}(\phi, x))$. As in the derivation of (6.7), it follows that for $0 < \tau < T_A$, $h(x, \tau)$ can be approximated as

$$h(x, \tau) \;=\; \hat{h}_{FP}(\phi, x) + (h_0 - \hat{h}_{FP}(\phi, x))e^{-\tau/\tau_L}.$$

When the active group of cells makes the jump down, some inhibited group of cells will jump from left to right. All the cells such that $h(x, T_A) > h_{LK}(0)$ will make the jump. Only a group of size ϕ can jump, so that cells for $x > \phi$ must be below the left knee while those for which $0 < x < \phi$ must be above the left knee. Thus, we have the threshold condition

$$h(\phi, T_A) \equiv \hat{h}_{FP}(\phi, \phi) + (h_0 - \hat{h}_{FP}(\phi, \phi))e^{-T_A/\tau_L} \;=\; h_{LK}(0). \tag{6.11}$$

This gives a formula for ϕ.

Remark. In the derivation of this formula, we assumed that cells remain synchronized as they jump up to the active phase. This requires that the synaptic activation is slower than the jumping up process. One way to achieve this is to consider *indirect synapses* as in [13]; this introduces a small, but $O(1)$ with respect to ϵ, delay from the time a cell fires until the corresponding synapse begins to activate.

In fact, generically, there will be either two or no roots to (6.11). To see why, note that $h_{FP}(S)$ is a monotonic function of S since as S increases, the v-nullcline rises and thus $h_\infty(v)$ will increase since v is decreasing. The function $S(\phi) \equiv s_{tot}(\phi, \phi)$, on the other hand, is shaped like an inverted parabola: clearly $S(0) = 0$, and $S(\phi)$ then increases as ϕ increases, reaches a maximum, and thereafter decays toward 0 as ϕ is increased further. If $W(x)$ has compact support, then $S(\phi)$ will vanish for $\phi > \phi_{max}$. Since $h_{FP}(S)$ is monotone increasing and $S(\phi)$ is shaped like an inverted parabola, it follows from (6.11) that

$$h(\phi, T_A) \equiv h_{FP}(S(\phi))[1 - e^{-T_A/\tau_L}] + h_0 e^{-T_A/\tau_L}$$

is also shaped like an inverted parabola. Thus, if there are any roots at all, there will be a pair corresponding to a small ϕ_- and a large ϕ_+.

It is instructive to consider the effect of changing the synaptic conductance (g_{syn}). As the conductance increases, the function $h_{FP}(S)$ becomes steeper and rises to a larger value. Thus if we decrease the conductance, ϕ_- will increase while ϕ_+ will decrease. At sufficiently small conductance values, the two roots will merge. Numerically, we find that as the conductance is reduced, the pulse-width decreases in size. This leads us to conjecture that the stable branch of lurching solutions is the one corresponding to ϕ_+.

Note that if $T_A \ll \tau_L$, then $h(\phi, T_A) \approx h_0 < h_{LK}(0)$, so there will be no solution. Since T_A represents the length of the cell's active phase, this implies that lurching waves cannot arise in inhibitory networks of spiking neurons (whose active phases are very short) unless they are endowed with additional properties.

One can obtain a simple bound on T_A if we assume that (A2) is satisfied. Then T_A satisfies (6.4) where h_J is the value of h where the cells jump up. Since $h_{LK}(0) < h_J < h_{FP}(1)$, we conclude that

$$\tau_R \ln \frac{h_{LK}(0)}{h_{RK}(1)} < T_A < \tau_R \ln \frac{h_{FP}(1)}{h_{RK}(1)}.$$

7. Discussion. We have discussed a variety of waves that are found in inhibitory thalamic networks endowed with rebound behavior. The analysis we develop leads to implicit formulas describing how the velocity of the waves relates to network parameters. The geometric constructions of singular smooth and lurching waves are quite similar. In both cases, cells lie along the left branch of some cubic-shaped curve while silent and along a right branch while active. Cells on a left branch must be able to escape from the silent phase—that is, reach a left knee—in order to jump up to the active phase. If the cells are excitable at all levels of synaptic input, then silent cells must first be released from inhibition before they can escape. The generation of smoothly propagating waves is impossible if the connectivity is on-centered; a smooth wave can exist only if the synaptic footprint is off-centered, and cells are released when they enter the region corresponding to the gap in the effective input. In the case of lurching waves, cells are released from inhibition only after the preceding cluster of active cells returns to the silent phase.

Distinguishing whether or not cells are able to escape the silent phase leads to conditions on parameters for when a particular wave exists. Supposing that each cell is excitable for all levels of synaptic input, then a traveling wave cannot exist if g_{syn} is too small. The geometric reason for this is that with very small g_{syn}, the fixed point on the cubic corresponding to maximal inhibitory input lies below the left knee of the cubic corresponding to zero inhibitory input. This argument also explains why a lurching wave cannot exist if the parameter τ_R is too big, that is, in the case of spiking neurons. For both smooth and lurching waves, a small value of β, i.e., a very slow rate of synaptic deactivation, makes escape impossible. Escape will be possible provided both β and g_{syn} are sufficiently large.

Note that in the case of lurching waves, cells must wait in the silent phase for the preceding cluster of active cells to jump down and release them from inhibition. There is therefore a delay from when a cell first starts to receive inhibition to when that cell begins to be released from the inhibitory influence. During this delay period, cells within the inhibited cluster approach the fixed point along their associated left branch. This results in a compression of the distance in phase space between these cells, which tends to synchronize cells within each cluster. Since with smooth waves the firing of cells is not contingent on presynaptic cells jumping down first, there is no such delay. Hence, there is less compression of the distances between cells, and the cells are thus able to jump up in a continuous fashion.

Our results complement those of Golomb and Ermentrout [7] in which simple models of neurons with excitatory coupling and coupling delay were studied. In the context of the thalamic RE-TC network, the neurons in [7] correspond to the RE cells which effectively send excitatory coupling to other RE cells through interactions with the TC cells. The coupling delay is due to the time needed for post inhibitory rebound of the TC cells, as well as the long active phases of the RE cells. It is shown in [7] that for the specific example of integrate and fire neurons, a smooth wave becomes unstable if the coupling delay becomes large enough. In the present paper, we view the neurons in a single-layered network as corresponding to the TC

cells which effectively send inhibition to other TC cells through interactions with the RE cells. Since an inhibited cell with the rebound property must wait a prescribed amount of time for the inhibitory influence on it to wear off before firing, effectively it cannot fire until a fixed delay passes. If this delay can be shortened, then smooth waves are expected. One advantage of the approach we take in this paper is that the coupling delay emerges from the geometric analysis and is not specified a priori.

Our analysis has been for one-layered networks. However, the numerical results clearly demonstrate that both smooth and lurching waves exist in two-layered networks and the geometric approach certainly generalizes to this case. It is interesting to compare the lurching waves illustrated in [12], which were generated from a single-layered network, with those illustrated here, which were generated from a double-layered network. The wakes of the lurching waves shown in Figure 5 are much more organized than those shown in [12]. In Figure 5(c), for instance, cells in the wave's wake break up into different synchronized clusters that take turns firing. Distinct clusters with fixed membership of cells have not been observed to form in the wake of the lurching waves in [12]. In a two-layered network, the cells of the layer corresponding to TC cells must wait in the silent phase until cells of the second layer, corresponding to RE cells, jump down and release them from inhibition. If the active phase of the RE cells is quite long, there would be strong compression among the TC cells receiving inhibition in the silent phase. This strong compression would lead to more synchronized clusters in the wake of the lurching wave. We remark that, by adjusting the length of the RE cells' active phase, it is much easier to control the degree of compression in a two-layered network than in a one-layered array. A more detailed discussion comparing synchronization and compression mechanisms in one- and two-layered networks is given in [13].

A given network may display other types of propagating activity patterns besides the smooth and lurching waves described here. Bistable patterns that exist for the same set of parameter values may also be possible. For example, in [12] a saltatory wave is shown which lurches in one direction and each new active cluster leaves a smooth wave in its wake. Although the behavior of this solution in one direction is very different from that in the other direction, the underlying network is completely homogeneous and symmetric; the only asymmetry is in the initial data. By choosing the initial conditions appropriately it may be possible to generate a periodic smooth wave within the same parameter regime. A more complete discussion of such bistability issues is beyond the scope of this paper.

The integral-differential equations studied here resemble reaction-diffusion systems such as the FitzHugh–Nagumo equations. We remark that the speed of a traveling wave solution of a reaction-diffusion system is usually determined by the fast jumping up process. This contrasts sharply with the waves studied here, for which the velocities are determined by the slow dynamics, intrinsic and synaptic. In the geometric singular perturbation framework, we reduce the analysis of the full system to studying equations for just the slow variables. These slow subsystems often consist of first-order, scalar equations; for this reason, we were able to derive formulas for the wave speed. Such formulas are typically impossible to find for reaction-diffusion systems.

We have not addressed the issue of stability of the waves in the present paper. This is a difficult problem. Our numerical results indicate that in cases where there are two possible velocities, the slower wave is usually the stable one. This is in contrast to integrate and fire models as well as other models of excitation-driven waves, for

which the faster waves are stable. Finally, we have only looked at one-dimensional propagation. An interesting question is whether or not lurching waves exist in two-dimensional arrays, and if so, what do they look like? Preliminary numerical results suggest the possibility of lurching target waves. This is an open area to explore.

Appendix. Here we present various equations and formulas which are not in the body of the text. The nonlinear functions $m_\infty(v)$ and $h_\infty(v)$ of (2.1) are assumed to take the same general form. In addition, a function $s_\infty(v)$ also of that form was used to approximate the Heaviside function $H(v-\theta)$ when numerically integrating (2.3) or (2.4). Specifically, letting $X = m$, h, or s, we have $X_\infty(v) = [1+\exp(-(v-\theta_X)/\sigma_X)]^{-1}$. The remaining nonlinear function $\tau_h(v)$ in (2.1) is defined by $\tau_h(v) = \tau_R + (\tau_L - \tau_R)/[1+\exp(-(v-\theta_{h\tau})/\sigma_{h\tau})]$.

The smooth waves in Figures 8–11 were found in the following parameter regime. Fixed values were $g_L = 0.4, v_L = -70, g_{Ca} = 1.5, v_{Ca} = 90, v_{syn} = -85, \theta_m = -40, \sigma_m = 7.4, \theta_h = -70, \sigma_h = -4, \theta_{h\tau} = -50, \sigma_{h\tau} = -3$. For the synaptic footprint we used a function $W(x)$ defined as

$$W(x) = \begin{cases} \frac{1}{2\sigma} & : \quad \gamma < |x| < 1, \\ 0 & : \quad \text{otherwise}, \end{cases}$$

where $\sigma = 1-\gamma$. For direct numerical integration of the integral-differential equations (dashed curves in Figures 8 and 9), we also took $\alpha = 1, \theta_s = -35, \sigma_s = 2$, and initiated the wave with a localized small perturbation (either depolarizing or hyperpolarizing) from the resting potential ($v_0 \approx -65.57$). In our computations based on the two-point boundary value problem (solid curves in Figures 10–11), we took $\lambda = 5.58, \epsilon = 0.1$ as default values, but it turns out that at least for $0.05 \le \epsilon \le 2$ and $3 \le \lambda \le 6.1$ the values of these parameters have little effect on the results. For the parameters we varied, the default or starting values were $g_{syn} = 2.5, \beta = 0.025, \sigma = 0.5, \tau_R = 30, \tau_L = 830$. We initialized the AUTO continuation process using the following values for the wave speed and pulse-width: $c = 0.0018, a = 0.21125$. In both types of computation (boundary value problem or integral-differential system), an extra factor δ was inserted in front of the h vector field. This has the effect of scaling $\tau(v)$. Our curves were obtained with $\delta = 0.25$.

We present here a few salient facts about the $S_{tot}(\xi; c, a)$ calculated from (5.2)–(5.3) and a footprint $W(x)$ of the form described in the previous paragraph. Since we do not analyze the wake of the smooth wave in this paper, we shall only be concerned with behavior up until the jump-up occurring at $\xi = 0$. For $\xi \le 0$, S_{tot} is described by the following formulas: $S1 = \frac{1}{2\sigma}(1+\xi)$, $S2 = \frac{1}{2\sigma}\{\frac{c}{\beta}[1-e^{\frac{\beta}{c}(a-\xi-1)}]+a\}$, $S3 = \frac{1}{2}$, $S4 = \frac{1}{2\sigma}\{\frac{c}{\beta}[1-e^{\frac{\beta}{c}(a-\xi-1)}]+(a-\gamma-\xi)\}$, or $S5 = \frac{1}{2\sigma}\cdot\frac{c}{\beta}\{e^{\frac{\beta}{c}(a-\xi-\gamma)} - e^{\frac{\beta}{c}(a-\xi-1)}\}$. Which form S_{tot} takes depends on the relative sizes of a, γ, σ, as well as on the value of ξ. From the above expressions for $S_{tot}(\xi; c, a)$, we find $S_{tot}(0; c, a)$ to be

$$S_{tot}(0;c,a) = \begin{cases} \frac{1}{2\sigma}\cdot\frac{c}{\beta}e^{\frac{\beta}{c}(a-\gamma)}\left\{1-e^{-\frac{\beta}{c}\sigma}\right\} & \text{if } a < \gamma, \\ \frac{1}{2\sigma}\left\{\frac{c}{\beta}\left[1-e^{\frac{\beta}{c}(a-1)}\right]+(a-\gamma)\right\} & \text{if } \gamma < a < 1, \\ \frac{1}{2} & \text{if } a > 1. \end{cases}$$

Also, one can see that S_{tot} reaches a maximum at $\xi = -\gamma$, and this peak value is

$$S_{tot}(-\gamma;c,a) = \begin{cases} \frac{1}{2\sigma}\left\{\frac{c}{\beta}\left[1-e^{\frac{\beta}{c}(\gamma+a-1)}\right]+a\right\} & \text{if } a < 1-\gamma, \\ \frac{1}{2} & \text{if } a > 1-\gamma. \end{cases}$$

For the lurching waves in Figure 14, the following parameter values were used. Fixed values were $g_L = 0.1, v_L = -60, g_{Ca} = 1.5, v_{Ca} = 90, v_{syn} = -95, \theta_m = -40, \sigma_m = 7.4, \theta_h = -78, \sigma_h = -2, \theta_{h\tau} = -50, \sigma_{h\tau} = -3, \tau_R = 100$. For numerical integration of the network equations (2.3) (dashed curves in Figure 14), we also took $\alpha = 2, \theta_s = -35, \sigma_s = 2$, and initiated the wave with a slight depolarization from the rest state (which has $v_0 \approx -60$). In this parameter regime, a lurching wave was observed in the simulations when we set self-inhibition to be zero, i.e., each cell in the model (representing a cluster of cells physically) inhibits its immediate neighbors but not itself. Therefore, for consistency, in our calculations based on the analytic formulas (6.6)–(6.8) we used $h_{RK}(0)$ instead of $h_{RK}(\phi)$ and took $h_{FP}(\phi) = h_{FP}(1)$. All arguments presented in section 6.2 are just as valid in this situation of off-centered connectivity. For these formula-based calculations (solid curves in Figure 14) we also took $\lambda = \mu\, g_{syn}$, and the constant of proportionality μ was chosen to be 6.25. For the parameters we varied, the starting values were $g_{syn} = 0.4, \beta = 0.05$, and $\tau_L = 200$.

Each wave shown in Figures 4 and 5 is a solution of a two-layered network as illustrated in Figure 1. Every cell without any coupling satisfies a system of the form (2.1). The nonlinear functions $m_\infty(v), h_\infty(v)$, and $\tau_h(v)$ are defined as above. The coupling between RE and TC cells is modeled as follows. To the voltage equation of the jth TC cell we add the term $g^T_{syn} s_\infty(v^j_{RE})(v^j_{TC} - v^T_{syn})$. Here v^j_{RE} is the voltage of the jth RE cell and v^j_{TC} is the voltage of the jth TC cell. To the voltage of the jth RE cell, we add the term

$$\frac{1}{2\omega} g^R_{syn}(v^j_{RE} - v^R_{syn}) \sum_{i=j-\omega}^{j+\omega} s_\infty(v^i_{TC}).$$

So each TC cell receives input from precisely one RE cell, while each RE cell receives input from a set of TC cells with square footprint of size determined by ω. For simplicity, we use instantaneous synapses.

For each solution shown in Figures 4 and 5, the network consisted of 75 TC cells and 75 RE cells, with $\omega = 6$. Fixed values corresponding to each TC cell were $g_L = .01, v_L = -75, g_{Ca} = 1, \theta_m = -65, \sigma_m = 7.8, \theta_h = -79, \sigma_h = 5, \tau_R = 1, \tau_L = 80, \theta_{h_\tau} = -65, \sigma_{h_\tau} = 4$. Fixed values corresponding to each RE cell were the same as for the TC cells with the exception of $g_L = .2, v_L = -80$. Also fixed were $\theta_s = -20, \sigma_s = 2, v^T_{syn} = -80, v^R_{syn} = 0$. In Figure 4, $v_{Ca} = 120$. The values of ϵ for the TC and RE cells in Figures 4(a), 4(b), and 4(c) were $(1, 1), (2, .6)$, and $(2, .36)$, respectively. The values of (g^T_{syn}, g^R_{syn}) were $(.03, .1)$, $(.1, .1)$, and $(.1, .1)$, respectively. In Figure 5, $v_{Ca} = 90$, $g^T_{syn} = .1$, and $g^R_{syn} = .3$. The values of ϵ for the TC and RE cells in Figures 5(a), 5(b), and 5(c) were $(3, 1), (5, 1.01)$, and $(3, .5)$, respectively.

Acknowledgment. We thank the referees for their many useful suggestions and comments.

REFERENCES

[1] T. Bal, M. von Krosigk, and D.A. McCormick, *Synaptic and membrane mechanisms underlying synchronized oscillations in the ferret lateral geniculate nucleus in vitro*, J. Physiol. Lond., 483 (1995), pp. 641–663.

[2] T. Bal, M. von Krosigk, and D.A. McCormick, *Role of ferret perigeniculate nucleus in the generation of synchronized oscillations in vitro*, J. Physiol. Lond., 483 (1995), pp. 665–685.

[3] M. Bazhenov, I. Timofeev, M. Steriade, and J. Sejnowski, *Self-sustained rhythmic activity in the thalamic reticular nucleus mediated by depolarizing GABA-A receptor potentials*, Nature Neurosci., 2 (1999), pp. 168–174.

[4] Z. Chen, B. Ermentrout, and X.-J. Wang, *Wave propagation mediated by GABAB synapse and rebound excitation in an inhibitory network: A reduced model approach*, J. Comput. Neurosci., 5 (1998), pp. 53–69.

[5] A. Destexhe, T. Bal, D.A. McCormick, and T.J. Sejnowski, *Ionic mechanisms underlying synchronized oscillations and propagating waves in a model of ferret thalamic slices*, J. Neurophysiol., 76 (1996), pp. 2049–2070.

[6] E.J. Doedel, A.R. Champneys, T.F. Fairgrieve, Y.A. Kuznetsov, B. Sandstede, and X. Wang, Auto97: *Continuation and Bifurcation Software for ODEs (with* homcont*)*, Technical Report, Concordia University, 1997.

[7] D. Golomb and B. Ermentrout, *Continuous and lurching traveling pulses in neuronal networks with spatially-decaying connectivity and delay*, Proc. Natl. Acad. Sci. USA, 96 (1999), pp. 13480–13485.

[8] D. Golomb, X.-J. Wang, and J. Rinzel, *Propagation of spindle waves in a thalamic slice model*, J. Neurophysiol., 75 (1996), pp. 750–769.

[9] U. Kim, T. Bal, and D.A. McCormick, *Spindle waves are propagating synchronized oscillations in the ferret LGNd in vitro*, J. Neurophysiol., 84 (1995), pp. 1301–1323.

[10] U. Kim and D.A. McCormick, *The functional influence of burst and tonic firing mode on synaptic interaction in the thalamus*, J. Neurosci., 18 (1998), pp. 9500–9516.

[11] D. Pinault and M. Deschenes, *Anatomical evidence for a mechanism of lateral inhibition in the rat thalamus*, Eur. J. Neurosci., 10 (1998), pp. 3462–3469.

[12] J. Rinzel, D. Terman, X.-J. Wang, and B. Ermentrout, *Propagating activity patterns in large-scale inhibitory neuronal networks*, Science, 279 (1998), pp. 1351–1355.

[13] J. Rubin and D. Terman, *Analysis of clustered firing patterns in synaptically coupled networks of oscillators*, J. Math. Biol., to appear.

[14] M. Steriade, D.A. McCormick, and T.J. Sejnowski, *Thalamocortical oscillations in the sleeping and aroused brain*, Science, 262 (1993), pp. 679–685.